SELF-PROPELLED INTERACTING PARTICLE SYSTEMS WITH ROOSTING FORCE

J. A. CARRILLO, A. KLAR, S. MARTIN, S. TIWARI

Abstract. A model for self-propelled interacting particles is extended and investigated. An attraction force to a roosting area is introduced and added to the particle system. Additionally to patterns like single mills, new scenarios of collective behavior are observed. The resulting equations are investigated analytically looking at different asymptotic limits of the corresponding stochastic model and at the hydrodynamic moment system. Numerical results and examples for microscopic and hydrodynamic equations are presented.

1. Introduction

Interacting particle systems have been widely used for the description of coherent motion of animal groups as schools of fish, flocks of birds or swarms of insects as well as bacterial growth at cellular level. All these groups are able to organize themselves in the absence of a leader allowing order to arise starting from disordered configurations [CDFSTB03, PE99, BDT99]. These systems are usually described by discrete models [VCBCS95, GC04, CKFL05, CKJRF02] in which some basic rules for modeling animal sociological behavior are included such as the social tendency to produce grouping, the inherent minimal space they need to feel comfortably inside the group and the mimetic adaptation to a group. Models including these three effects: attraction, repulsion, and orientation, are usually called 3-zone models that have widely been used for fishes [HW92, BTTYB09, BEBSVPSS09, KH03, HK05] and birds [BCCCCGLOPPVZ09, HCH]. Some minimal models have also been proposed to describe these phenomena by interacting agents using self-propelling forces, in which the only mimetic part of the model is the tendency towards a constant speed movement, and pairwise attractive and repulsive potentials, see [LRC00, DCBC06, CHDB07, CDMBC07, LLE08a, LLE08b]. Various collective configurations like invariant flocks, rotating mills, rings and clumps have been observed, studied, and classified.

As the number of particles grows, more compact approaches than tracing the path of each individual become increasingly desirable. For example, kinetic (mean-field) mesoscopic [DM08, HT08, HL09, CDP09, CFRT09, CCR09] and continuum macroscopic models [TT95, MEBS03, TB04, TBL06,

Date: January 29, 2010.

Key words and phrases. self-propelled interacting particles, roosting force, self-organization, diffusive limits, hydrodynamic limits, mean field equations.

BCM07] have recently been derived and investigated. These equations describe the evolution of averaged quantities like the probability density function, density or mean velocity of the particles. These models are to a certain extent able to approximate the microscopic dynamics. However, there might be cases where the fullness of the microscopic solution is not captured by the macroscopic one, see [CDP09]. We refer to [CDP09, CCR09] for a description of the transition from a microscopic modeling of swarming, to a continuum description via kinetic theory. We finally refer to [CFTV10, CCR10] for recent surveys about these different swarming models.

The above mentioned models are minimal in the sense that they aim at describing the basic patterns of self-organization phenomena. However, these models have to be extended by including other effects through forces and parameters to capture the behavior of specific groups of animals. For example, to describe the behavior of aerial displays of birds, typically a force called the roosting force becomes important, we refer to [HCH, BCCCCGLOPPVZ09] and references therein. This force describes the preference of the birds to stay over a 'roosting area'.

Including such additional forces leads to a better understanding of these aerial displays and to new collective configurations. The purpose of the present paper is to investigate a self-propelled interacting particle system where such a roosting force is included considering microscopic, kinetic and hydrodynamic descriptions and their respective derivations and to compare them numerically.

The paper is organized as follows: In section 2 we revise the standard model for self-propelled swarms including a roosting behavior. Moreover, the associated mean field equation is discussed. In section 3 a random noise is included in the model. Moreover, a model with constant velocities is motivated looking at the original system in polar coordinates. For these models we consider various asymptotic limits: different strength of the interaction and roosting forces are considered and diffusive and hyperbolic limits are discussed. In section 4 the hydrodynamic limit and associated milling solutions are considered for the model in section 2. An integral equation for single mills including the roosting force is derived. Section 5 is devoted to numerical experiments for the microscopic and hydrodynamic equations.

2. Self-propelled interacting particles with attraction-repulsion and roosting

To begin with, we consider the attraction-repulsion model of N interacting, self propelled particles with friction in $\mathbb{R}^d$ governed by the equations of motion

$$\begin{aligned}\frac{dx_i}{dt} &= v_i \\ \frac{dv_i}{dt} &= \alpha v_i - \beta v_i |v_i|^2 - \nabla_{x_i} \sum_{i \neq j} U(|x_i - x_j|)\end{aligned}$$

where U is an interaction potential and α, β are effective values for propulsion and friction forces, see [LRC00, DCBC06, CDMBC07]. A common choice is the Morse potential

$$U(r) = -C_a e^{-r/l_a} + C_r e^{-r/l_r}$$

which we will use for our computational examples. C_a, C_r are attractive and repulsive strengths and l_a, l_r are their respective length scales. Various patterns of self-organization emerge and have been categorized in [DCBC06]. Flocks, where particles tend to move at constant density and velocity, and milling solutions, where rotatory states are formed are of particular interest, see e.g. [LRC00, CDMBC07, CDP09, LLE08a]. These equations are extended by including an additional force, called the roosting force, describing an attraction to a roosting area or site. Big groups of birds move in collective swarms, which often tend to overfly a fixed preferred location (e.g. nesting area or a food source). Such a roosting force can be modeled in different ways, see, for example, [HCH, BCCCCGLOPPVZ09]. For simplicity we restrict ourselves to the two-dimensional case $d = 2$ and assume that the roosting site is at the origin. Similar to [HCH] one may then model this individual force with the term

$$F^1_{\text{Roost}} = -\operatorname{sgn}(v_i^\perp \cdot x_i) \left(1 + \frac{v_i \cdot x_i}{|v_i||x_i|}\right) \frac{v_i^\perp}{|v_i|}.$$

Here, $v_i^\perp$ denotes the normal to the velocity direction. The force is always directed orthogonal to the velocity of the particles giving each particle a tendency towards the origin. In this case, the roosting force is maximal, if the particles are directed away from the origin and equal to zero if they are directed towards the origin. The sign term is necessary in order not to prefer one sense of rotation for particles directed away from the origin over the other and induces the correct rotation sense as discussed below. Alternatively, we may consider the force

$$F^2_{\text{roost}} = -\left[v_i^\perp \cdot \nabla\phi(x_i)\right] v_i^\perp,$$

or normalized versions of it. In this case the roosting force is assumed to be proportional to $\nabla\phi(x_i) \cdot v_i^\perp$ giving the particles again a tendency towards the origin, if ϕ is suitably chosen. The roosting potential ϕ is a function $\phi : \mathbb{R}^2 \to \mathbb{R}$ with the generic example $\phi(x) = |x|^2/2$. For such a definition the roosting force is maximal if the particles are directed orthogonal to the direction to the origin. The induced sense of rotation for particles directed away from the origin is correct, in the sense that it is positive if the inner angle between the position vector and velocity vector is positive and vice versa. Therefore, we get rid of the sign term. In figure 1, we illustrate individual motion for the system without interaction forces. The first model yields a circular motion, whereas the second model gives a more involved pattern with changing radii around the origin. In the following, we concentrate on the second version of the roosting force. Compare [GKMW07, BGKMW07, KRS07] for a different

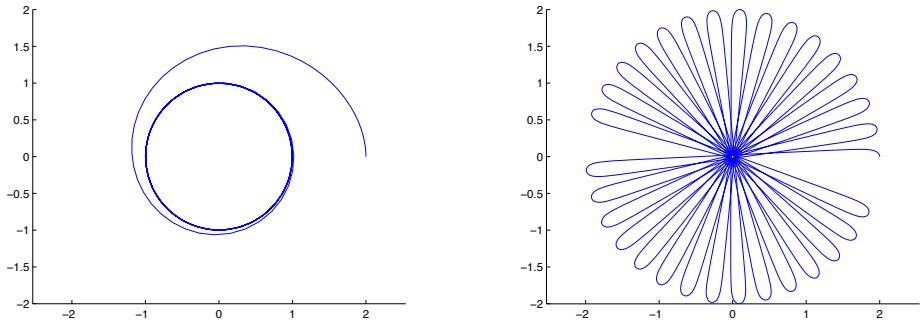

(a) F^1_{Roost} with initial particle $x = (2,0)^T, v = (0,0.5)^T$.

(b) F^2_{Roost} with roosting potential 2.1 and parameters $R_{\text{Roost}} = b = 1$

Figure 1: Examples of fundamental motion induced by the roosting forces on an individual particle.

application of such a forcing term to fiber lay down processes and [HCH] for an extensive biological modeling of swarming behavior. In order to intensify the roosting force outside a certain area and to diminish it therein, we henceforth use the roosting potential

$$\phi(x) := \frac{b}{4}\left(\frac{|x|}{R_{\text{Roost}}}\right)^4 \tag{2.1}$$

where R_{Roost} is the roosting radius and b is a constant weight.

By using the so-called 'weak coupling scaling' assumption [Dou79, Neu77, BH77, Spo91], one rescales the interaction potential with the factor $\frac{M}{N}$ where M denotes the fixed total mass. It will be normalized without loss of generality from now on to $M = 1$. Letting then N go to infinity, one can derive in the limit of a large number of particles the associated mean field equation [Dou79, Spo91, CDP09, CCR09]. Thus, our scaled microscopic model states

$$\begin{aligned} \frac{dx_i}{dt} &= v_i \\ \frac{dx_i}{dt} &= v_i(\alpha - \beta|v_i|^2) - \frac{1}{N}\nabla_{x_i}\sum_{i\neq j} U(|x_i - x_j|) \\ &\quad -v_i^{\perp}\,\nabla_{x_i}\left[\phi(x_i)\cdot v_i^{\perp}\right]. \end{aligned} \tag{2.2}$$

In figure 2, we illustrated the effect of the new force. With the introduction of roosting, patterns like mills can still be observed, but also new phenomena like local flocks traveling on circular curves ("milling flocks") are observed. Further details are presented in section 5.

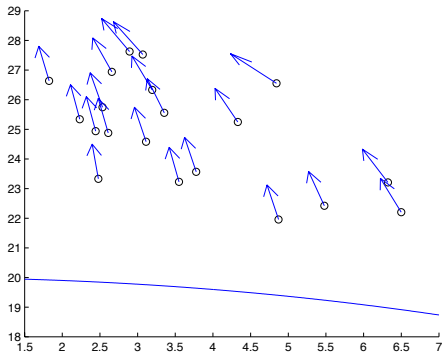

Figure 2: The roosting force: A flock of particles traveling at direction $(0,1)^T$ has crossed the roosting area and particles have started to rotated back to the origin. ($N = 20, R_{\text{roost}} = 20, b = \frac{1}{20}$, no interaction).

For N going to infinity one obtains the mean field equation for the distribution function $f = f(x, v, t)$ of the particles:

$$\partial_t f + v \cdot \nabla_x f + Sf = 0 \tag{2.3}$$

with force term

$$\begin{aligned} Sf &= \nabla_v \cdot \big(v(\alpha - \beta|v|^2)f\big) - \nabla_v \cdot ((\nabla_x U \star \rho)f) \\ &\quad -\nabla_v \cdot \left(\left[\nabla_x \phi \cdot v^\perp\right] v^\perp f\right), \end{aligned} \tag{2.4}$$

where the density ρ is defined as usual by

$$\rho = \int f dv \qquad \text{with } \int \rho \, dx = M = 1.$$

Let us mention that the rigorous passage from the microscopic particle system (2.2) towards the kinetic mean-field equation (2.3) as $N \to \infty$ is a particular case of the theory of well-posedness in measures for the kinetic equation (2.3) developed in [CCR09]. To be more precise, assuming that the roosting potential and the interaction potential are locally Lipschitz, then the sequence of particle solutions constructed as Delta Dirac sums out of (2.2) converges towards a solution of the kinetic mean-field model (2.3). This roosting force is an interesting case for the theory developed in [CCR09] compared to the classical theory in [Dou79, Spo91] since it is not a globally Lipschitz force in phase space.

3. Stochastic and constant velocity models and their asymptotic limits

In this section we extend the system to include a stochastic noise term. Moreover, a model for interacting particles with constant velocities is motivated. Different scalings and asymptotic limits for these models are considered.

3.1. **Random noise.** Adding a random noise to the system and redefining the propulsion and friction coefficients depending on the strength of the random noise A, the resulting stochastic differential system reads

$$\begin{aligned} \mathrm{d}x_i &= v_i\,\mathrm{d}t \\ \mathrm{d}v_i &= v_i(\gamma_1-\gamma_2|v_i|^2)dt - \frac{1}{N}\nabla_{x_i}\sum_{i\neq j}U(|x_i-x_j|)dt \\ &\quad -v_i^{\perp}\left[\nabla\phi(x_i)\cdot v_i^{\perp}\right]dt - \frac{A^2}{2}v_i dt + A\,\mathrm{d}W_t. \end{aligned} \tag{3.1}$$

One can obtain the mean-field equation for the distribution function $f = f(x,v,t)$ of the particles formally by Ito's calculus as in [Ri89] or rigorously as in [Szn91, BCC]:

$$\partial_t f + v\cdot\nabla_x f + Sf = Lf \tag{3.2}$$

with force term S as above and diffusive part

$$Lf = \frac{A^2}{2}\nabla_v\cdot\left(vf+\nabla_v f\right). \tag{3.3}$$

3.2. **Constant velocity model.** We rewrite the above stochastic system using Ito's calculus in polar coordinates $v_i = c_i\tau_i = c_i\tau(\alpha_i)$ with $c_i\in\mathbb{R}^+$ and $\tau = \tau(\alpha) = (\cos\alpha,\sin\alpha)^T$:

$$\begin{aligned} \mathrm{d}x_i &= c_i\tau_i\,\mathrm{d}t \\ \mathrm{d}c_i &= c_i(\gamma_1-\gamma_2|c_i|^2)dt - \frac{1}{N}\tau_i\cdot\nabla_{x_i}\sum_{i\neq j}U(|x_i-x_j|)dt \\ &\quad -\frac{A}{2}(c_i-\frac{1}{c_i})dt + A\,\mathrm{d}W_t \\ \mathrm{d}\alpha_i &= -c_i\tau_i^{\perp}\cdot\nabla\phi(x_i)dt \\ &\quad -\frac{1}{N}\frac{1}{c_i}\tau_i^{\perp}\cdot\nabla_{x_i}\sum_{i\neq j}U(|x_i-x_j|)dt + \frac{A}{c_i}\,\mathrm{d}W_t. \end{aligned} \tag{3.4}$$

Since the tendency of the system in nature is to equilibrate the speed by the friction and self-propelling forces, we neglect the noise term in the speed equation and we assume that the speed is already stationary. This motivates the following model of constant velocity c:

$$\begin{aligned} \mathrm{d}x_i &= c\tau_i\,\mathrm{d}t \\ \mathrm{d}\alpha_i &= -c\tau_i^{\perp}\cdot\nabla\phi(x_i)dt \\ &\quad -\frac{1}{N}\frac{1}{c}\tau_i^{\perp}\cdot\nabla_{x_i}\sum_{i\neq j}U(|x_i-x_j|)dt + \frac{A}{c}\,\mathrm{d}W_t. \end{aligned} \tag{3.5}$$

The associated mean field equation for the distribution function $f = f(x,\alpha,t)$ can also be rigorously derived, see [Szn91, BCC], and is given by

$$\partial_t f + c\tau\cdot\nabla_x f + S_\alpha f = L_\alpha f \tag{3.6}$$

with force term

$$S_\alpha f = S_\alpha^R + S_\alpha^U = -c\partial_\alpha\left(\tau^\perp\nabla\phi f\right) - \frac{1}{c}\partial_\alpha\left(\tau^\perp\nabla_x U\star\rho f\right) \tag{3.7}$$

and diffusion operator

$$L_\alpha f = \frac{A^2}{2}\frac{1}{c^2}\partial_{\alpha\alpha} f \tag{3.8}$$

and

$$\rho = \int_0^{2\pi} f d\alpha. \tag{3.9}$$

3.3. **Asymptotic limits.** In this section we consider different asymptotic limits of the mean field equations considered in the last section. We investigate situations with large and small values for the noise amplitude, the interaction force and the roosting force. First diffusive limits with a rescaled time are considered and second a hyperbolic scaling without time rescale is investigated.

3.3.1. *The limit for large noise, small interaction and small roosting.* We rescale the operator L in (3.2) with $L \to L/\epsilon$ and consider a large time scale $t \to t/\epsilon$. Assuming $\gamma_1 = \gamma_2 = 1$ this gives

$$\epsilon\partial_t f + v\cdot\nabla_x f + Sf = \frac{1}{\epsilon}Lf \tag{3.10}$$

with

$$Sf = \nabla_v\cdot\left(v(1-|v|^2)f\right) - \nabla_v\cdot(\nabla_x U\star\rho f) - \nabla_v\cdot\left(\nabla_x\phi\cdot v_i^\perp v_i^\perp f\right)$$

and

$$Lf = \frac{A^2}{2}\nabla_v\cdot(vf + \nabla_v f).$$

Expanding $f = f_0 + \epsilon f_1 + \cdots$, we obtain to order 1 in ϵ, $Lf_0 = 0$ or $f_0 = \rho(x,t)M(v)$ with

$$M(v) = \frac{1}{2\pi}\exp(-|v|^2/2).$$

To order ϵ we have $v\cdot\nabla_x f_0 + Sf_0 = Lf_1$, and since

$$\begin{aligned} v\cdot\nabla_x f_0 + Sf_0 =& v\cdot\nabla_x\rho M + \rho\nabla_v\cdot\left(v(1-|v|^2)M\right) \\ &- \rho\nabla_v\cdot(\nabla_x U\star\rho M) - \rho\nabla_v\cdot\left(\nabla_x\phi\cdot v^\perp v^\perp M\right) \\ =& v\cdot\nabla_x\rho M + (2-5|v|^2+|v|^4)M \\ &+ v\cdot\nabla_x\phi M\rho + \rho v\cdot\nabla_x U\star\rho M \\ =& v\cdot(\nabla_x\rho + \rho\nabla_x U\star\rho + \nabla_x\phi M\rho) + (2-5|v|^2+|v|^4)M \end{aligned}$$

we obtain

$$f_1 = -\frac{2}{A^2}v\cdot(\nabla_x\rho + \rho\nabla_x U\star\rho + \nabla_x\phi\rho)\,M \tag{3.11}$$

$$+ \rho(\frac{|v|^2}{2} - \frac{|v|^4}{4})M.$$

Integrating (3.10) with respect to v gives to first order in ϵ

$$\partial_t \rho + \nabla_x \cdot \int v f_1 dv = 0. \tag{3.12}$$

Substituting (3.11) yields

$$\partial_t \rho - \frac{2}{A^2} \nabla_x \cdot (\nabla_x \rho + \rho \nabla_x U \star \rho + \nabla_x \phi \rho) = 0 \tag{3.13}$$

or

$$\partial_t \rho = \frac{2}{A^2} \nabla_x \cdot ((\nabla_x U \star \rho + \nabla_x \phi)\rho) + \Delta_x \rho. \tag{3.14}$$

We obtain a drift diffusion equation where the drift term is composed by an interaction term and a roosting term, compare [CDP09] for the case without roosting.

Remark 3.1. *For the constant velocity model a similar result is obtained in a straightforward way.*

3.3.2. *The limit for large angular noise, vanishing interaction and small roosting.* In this subsection we consider the constant velocity model (3.6). We rescale the operator L_α like $L_\alpha \to L_\alpha/\epsilon$, use again the diffusive time scale $t \to t/\epsilon$ and rescale the operators S_α^U like ϵS_α^U. Moreover, we fix $c = 1$. This leads to

$$\epsilon \partial_t f + \tau \cdot \nabla_x f - \partial_\alpha \left(\tau^\perp \nabla \phi f \right) - \epsilon \partial_\alpha \left(\tau^\perp \nabla_x U \star \rho f \right) = \frac{1}{\epsilon} L_\alpha f \tag{3.15}$$

To order 1 we get

$$f_0 = f_0(x) = \frac{\rho(x)}{2\pi}.$$

To order ϵ one obtains

$$\tau \cdot \nabla_x f_0 - \partial_\alpha \left(\tau^\perp \nabla \phi f_0 \right) = L_\alpha f_1 = \frac{A^2}{2} \partial_{\alpha\alpha} f_1 \tag{3.16}$$

or

$$f_1 = -\frac{2}{A^2} \tau \cdot (\nabla_x f_0 + \nabla_x \phi f_0) \tag{3.17}$$

Integrating (3.15) with respect to α gives

$$\epsilon \partial_t \int f d\alpha + c \nabla_x \cdot \int \tau f d\alpha = 0 \tag{3.18}$$

Up to order ϵ we obtain

$$\partial_t f_0 + \frac{1}{2\pi} \nabla_x \cdot \int \tau f_1 d\alpha = 0. \tag{3.19}$$

Inserting f_1 and computing the integral over the tensor product yields the following equation for ρ:

$$\partial_t \rho - \frac{1}{A^2} \nabla_x \cdot (\nabla_x \rho + \nabla_x \phi \rho) = 0. \tag{3.20}$$

This equation is equivalent to an equation derived in the context of fiber lay down processes in the limit of large turbulence of the surrounding air flow, compare [BGKMW07, HKMO09].

3.3.3. *The large angular noise and large roosting limit.* Finally, a hyperbolic limit without time rescale is investigated. We consider again equation (3.6) with $c = 1$ and the hyperbolic scaling $L_\alpha \to L_\alpha/\epsilon$ and $S_\alpha^R \to S_\alpha^R/\epsilon$. This gives

$$\partial_t f + \tau \cdot \nabla_x f - \frac{1}{\epsilon}\partial_\alpha \left(\tau^\perp \nabla\phi f\right) - \partial_\alpha \left(\tau^\perp \nabla_x U \star \rho f\right) = \frac{1}{\epsilon} L_\alpha f \tag{3.21}$$

To order 1 we have

$$-\partial_\alpha \left(\tau^\perp \nabla\phi f_0\right) = L_\alpha f_0 = \frac{A^2}{2}\partial_{\alpha\alpha} f_0$$

or

$$-\left(\tau^\perp \nabla\phi f_0\right) = \frac{A^2}{2}\partial_\alpha f_0. \tag{3.22}$$

Equation (3.22) is solved by

$$f_0(x,\alpha) = \frac{\rho(x)}{N(x)} \exp\left(-\frac{2}{A^2}\tau \cdot \nabla\phi\right) \tag{3.23}$$

with

$$N(x) = \int \exp\left(-\frac{2}{A^2}\tau \cdot \nabla\phi\right) d\alpha.$$

We integrate (3.21) over α and obtain up to order ϵ

$$\partial_t \rho + \nabla_x \cdot \int \tau f_0 d\alpha = 0 \tag{3.24}$$

This can be rewritten as

$$\partial_t \rho + \nabla_x \cdot (\rho V) = 0 \tag{3.25}$$

with

$$V = V(x) = \frac{1}{N(x)} \int \tau \exp\left(-\frac{2}{A^2}\tau \cdot \nabla\phi\right) d\alpha. \tag{3.26}$$

Assuming $\phi(x) = \phi(|x|)$ we have $N(x) = N(|x|)$ and we can rewrite V as

$$V(x) = \lambda(|x|)x$$

with

$$\lambda(|x|) = \frac{1}{\phi'(|x|)|x|N(|x|)} \int \nabla\phi \cdot \tau \exp\left(-\frac{2}{A^2}\tau \cdot \nabla\phi\right) d\alpha.$$

Thus, the limit equation is

$$\partial_t \rho + \nabla_x \cdot (\rho\lambda(|x|)x) = 0. \tag{3.27}$$

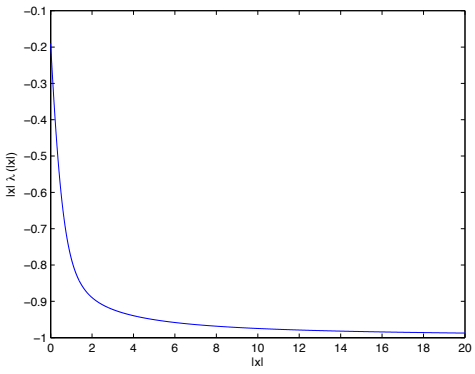

Figure 3: Plot of $|x|\lambda(|x|)$ for fixed $A = 1$ and $\phi(x) = \frac{|x|^2}{2}$.

Under suitable assumptions on ϕ, one shows that λ is negative, i.e. the velocity V points towards the origin with, $V(x) = 0$ for $x = 0$ as expected for the roosting force. For example, for $\phi(x) = |x|^2/2$ we have

$$|x|\lambda(|x|) = \frac{\int \cos\alpha \exp(-\frac{2}{A^2}\cos\alpha|x|)d\alpha}{\int \exp(-\frac{2}{A^2}\cos\alpha|x|)d\alpha}$$

which is a negative function with values in $(-1, 0)$ being 0 at $x = 0$, see figure 3.

4. Hydrodynamic limit and milling solutions

As in [CDMBC07, CDP09] for the equations without roosting force, one can derive hydrodynamic limits in the present case as well. Consider the mean field equation without diffusive part, i.e.

$$\partial_t f + v \cdot \nabla_x f + Sf = 0 \tag{4.1}$$

with

$$\begin{aligned} Sf =& \nabla_v \cdot \left(v(\alpha - \beta|v|^2)f\right) \\ & - \nabla_v \cdot (\nabla_x U \star \rho f) - \nabla_v \cdot \left(\nabla_x \phi \cdot v^\perp v^\perp f\right). \end{aligned} \tag{4.2}$$

Integrating against dv and $v\,dv$ and neglecting fluctuations gives the continuity equation

$$\partial_t \rho + \nabla_x \cdot (\rho u) = 0 \tag{4.3}$$

and the momentum equation

$$\partial_t u + (u \cdot \nabla_x)u = u(\alpha - \beta|u|^2) - \nabla_x U \star \rho - \left(u^\perp \otimes u^\perp \cdot \nabla_x \phi\right) \tag{4.4}$$

in the support of the density ρ. This is only true if fluctuations are neglected, i.e, for monokinetic distributions, compare [LRC00, CDMBC07, CDP09]. Equations (4.3,4.4) are numerically investigated and compared to the solution of the microscopic equation (3.1) without noise term in section 5.

Remark 4.1. *(Stationary distributions) Assuming $\beta|u|^2 = \alpha$ and the stationary case we obtain from the hydrodynamic equations above*

$$\nabla_x \cdot (\rho u) = 0 \tag{4.5}$$

$$(u \cdot \nabla_x)u = -\nabla_x U \star \rho - \left(u^\perp \otimes u^\perp \cdot \nabla_x \phi\right) \tag{4.6}$$

in the support of the density ρ. Assuming a rotatory solution given by

$$u = \sqrt{\frac{\alpha}{\beta}} \frac{x^\perp}{|x|},$$

compare [CDP09]*, and looking for radial densities $\rho = \rho(|x|)$, we obtain the continuity equation and*

$$(u \cdot \nabla_x)u = -\frac{\alpha}{\beta}\frac{x}{|x|^2} \tag{4.7}$$

$$-\frac{\alpha}{\beta}\frac{x}{|x|^2} = -\nabla_x U \star \rho - \frac{\alpha}{\beta}\frac{x}{|x|^2} x \cdot \nabla_x \phi \tag{4.8}$$

Assuming $\phi(x) = \phi(|x|)$ we end up with an integral equation for ρ:

$$U \star \rho = D + \frac{\alpha}{\beta}\left(\ln|x| - \phi(|x|)\right) \tag{4.9}$$

in the support of the density ρ. A numerical investigation of the stationary states is performed in the next section. With the same arguments as in [CDP09] *to each milling solution a double mill can be associated.*

5. Numerical experiments

In this section we present a series of numerical experiments on the microscopic equations (2.2), as well as the hydrodynamic limit (4.3,4.4). Different situations are studied and various patterns like single mills, milling flocks and interlaced rotations are investigated. In particular, the differences arising from the inclusion of the roosting force are considered. The microscopic equations are solved by a high order adaptive Runge-Kutta scheme for systems of ordinary differential equations. For a straightforward implementation, the complete distance matrix $(d_{i,j}) = |x_i - x_j|$ has to be computed in order to evaluate the interaction potential. Since this is costly, there is a restriction on the number particles which can be simulated in this way. Though $N = 1000$ are still possible to compute in reasonable time, we have used at most $N = 400$ particles in our examples, which seem to be sufficient. In order to simulate higher numbers of particles, one has to use more sophisticated algorithms. The hydrodynamic limit (4.3,4.4) is considered in detail numerically using a macroscopic particle method, see [TK07]. The macroscopic particle methods is based on a Lagrangian formulation of the hydrodynamic equations (4.3, 4.4). We consider

$$\begin{aligned} \partial_t x &= u \\ \partial_t \rho &= -\rho \frac{\partial u}{\partial x} \end{aligned}$$

$$\partial_t u \quad = \quad \alpha u - \beta |u|^2 u - \nabla_x U \star \rho - u^\perp u^\perp \cdot \nabla_x \phi.$$

One evaluates these quantities at the particle locations and approximates the spatial derivative of u by a difference approximation. The integral over the interaction potential is evaluated by a straightforward integration rule:

$$\nabla_x U \star \rho \sim \sum_j \nabla_x U(|x - x_j|)\rho_j dV_j$$

where dV_j is the local area around a particle determined by a nearest neighbour search. The resulting equations are then solved by a time discretization of arbitrary order. Diffusive terms can be included as well in a straightforward way. Obviously, this shows that the actual macroscopic computations are very similar to the microscopic ones. The difference lies in the way the interaction term is evaluated. In the microscopic case we compute

$$\frac{1}{N} \sum_j \nabla_x U(|x - x_j|)$$

instead of the above expression. If the values of ρ_j and dV_j are all equal then using

$$1 = \int \rho(x) dx \sim \sum_j \rho_j dV_j$$

it is easy to see that both simulations are equivalent to each other. However, in the macroscopic situation the particles are not physical particles as in the microscopic case. They play the role of discretization points. In particular, if the number of 'real' particles is very large, that does not mean that the number of macroscopic particles in the particle method has to be increased in the same way. The number of macroscopic particles is only chosen according to accuracy considerations. On the other hand, the macroscopic equations considered here are derived under the assumption of a mono-kinetic distribution function. Thus, they are not able to capture certain patterns like superimposed double mills, which are not described by a mono-kinetic distribution, see [CDP09].

5.1. **Numerical experiments with the microscopic system.** When comparing collective patterns of (2.2) with models without roosting, the first assertion is the disappearance of classical flocking: A state of particles steadily moving at constant relative distance and constant velocity is not possible in presence of roosting, since the roosting force quickly dominates other forces outside the roosting area, and turns particles back to origin. Secondly, we can preserve collective patterns where particles are moving in a fixed bounded area around the origin by strongly increasing the roosting radius, such that the roosting force never comes into play. Let us now look at single mill solutions. Consider a fixed set of interaction potential parameters, such that milling solutions can be observed in absence of roosting [DCBC06], with particles rotating on a radial interval $[r_l, r_u]$. For a roosting radius $R_{roost} > r_u$, a similar mill will appear again in presence of roosting,

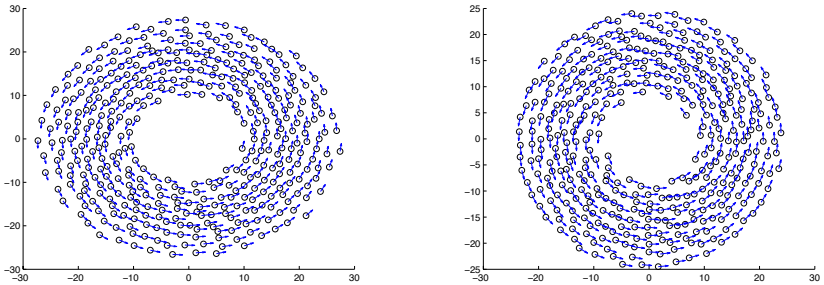

(a) no roosting

(b) $R_{\mathrm{Roost}} = 30$

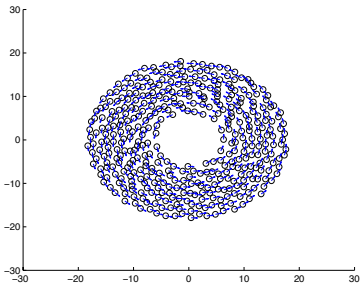

(c) $R_{\mathrm{Roost}} = 15$

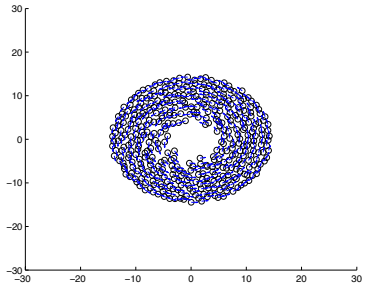

(d) $R_{\mathrm{Roost}} = 10$

Figure 4: Singular mills exists for the roosting force, their radial extend shrinks for decreasing roosting radii. (N=400, Interaction: $C_A = 20$, $C_R = 50$, $l_A = 100$, $l_R = 2$; Roosting : $b = \frac{1}{20}$; Propulsion : $\alpha = 0.07, \beta = 0.05$, velocity vectors are scaled for better visibility).

given suitable initial data. For $R_{roost} < r_u$, milling solution can still be observed. If they emerge, the mill is compressed. Figure 4 shows such singular mills with $[r_l, r_u] \approx [10, 30]$ and $R_{roost} = 30, 15, 10$. The corresponding radial densities are shown in the next subsection. Single mills for $R_{\mathrm{roost}} < r_u$ occur, but other patterns different from classical mills occur more often and are numerically more stable. Indeed, our simulations yield several collective states for identical set of parameters, when varying initial data. In figure 5, we illustrate typical patterns of collective behavior:

In (a), particles group in a local flock of common orientation and move collectively along a circular curve, so we have a "milling flock". In (b), we show the emergence of two distinct milling flocks. Another pattern is shown in (c): particles move in two interlaced circular flows at opposite direction. This pattern is can be considered a double mill, but it is not as symmetric and ordered as the single mills of figure 4.

Though a classification of initial data, parameters and resulting collective behavior is unclear at present state, our simulations show that interlaced rotations of figure 5(c) are more common than double mills in the pure

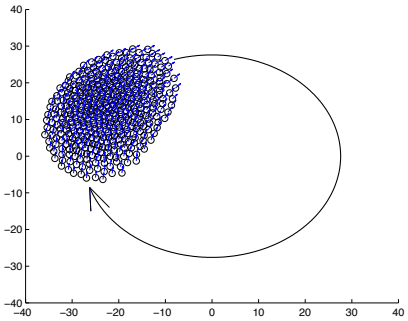

(a) Milling flock: Particles travel at common orientation along a circular curve ($N = 400$, $R_{\text{roost}} = 20$).

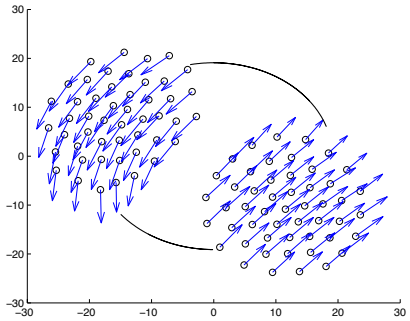

(b) Two milling flocks: Particles split into two groups along the same curve ($N = 100$, $R_{\text{roost}} = 30$).

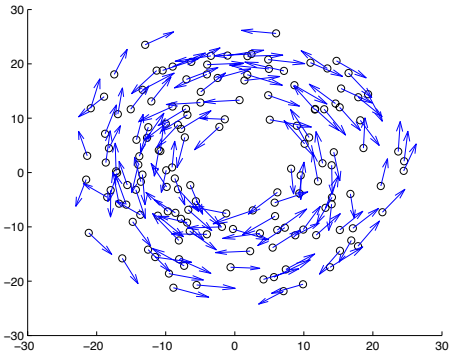

(c) Interlaced rotation: Two opposing circular flows emerge ($N = 400$, $R_{\text{roost}} = 20$).

Figure 5: Milling flocks and interlaced rotations as collective patterns of roosting (Interaction: $C_A = 20$, $C_R = 50$, $l_A = 100$, $l_R = 2$; Roosting : $b = \frac{1}{20}$; Propulsion : $\alpha = 0.07, \beta = 0.05$, velocity vectors are scaled for better visibility).

attraction-repulsion scenario. Also, transitions from seemingly stable interlaced rotation situations into milling flocks have been observed, but not vice versa. Since the roosting force is radially symmetric, all type of mills rotate around the origin as the central point, whereas in the pure attraction-repulsion case, single mills can form around other central points.

5.2. **Numerical investigation of the hydrodynamic limit.** In this subsection, we compare numerical results of hydrodynamic equations with densities obtained from microscopic simulation. The results for single mills are presented in figure 6. We can see, that hydrodynamics densities coincide

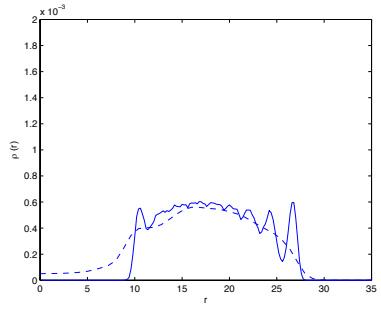

(a) No roosting, radial density

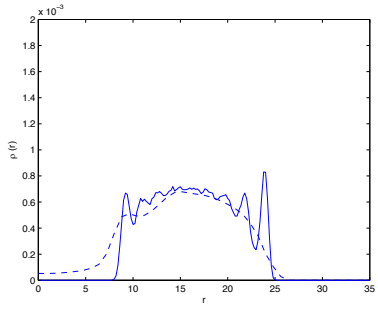

(b) $R_{\mathrm{Roost}} = 30$, radial density

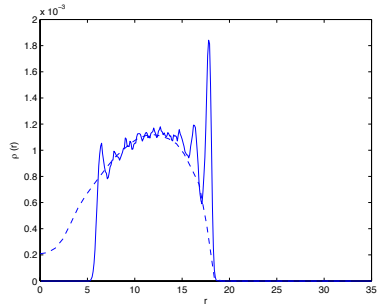

(c) $R_{\mathrm{Roost}} = 15$, radial density

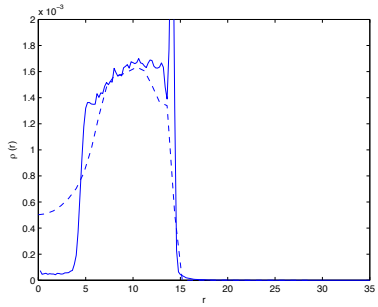

(d) $R_{\mathrm{Roost}} = 10$, radial density

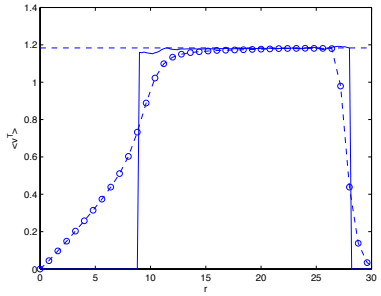

(e) No roosting, tangential velocity

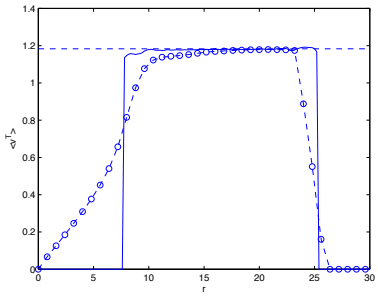

(f) $R_{\mathrm{Roost}} = 30$, tangential velocity

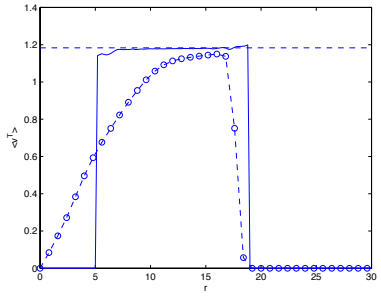

(g) $R_{\mathrm{Roost}} = 15$, tangential velocity

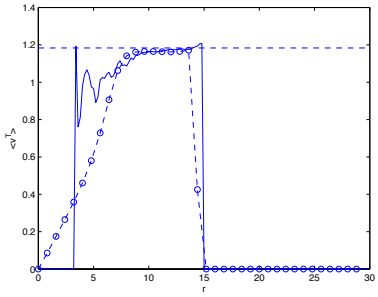

(h) $R_{\mathrm{Roost}} = 10$, tangential velocity

Figure 6: Comparison of microscopic and hydrodynamic radial densities and averaged tangential velocities. Densities: (-) microscopic, (--) hydrodynamic. Velocities: (-) microscopic, (--) equilibrium velocity, (-o) hydrodynamic. ($N = 400$, Interaction: $C_A = 20$, $C_R = 50$, $l_A = 100$, $l_R = 2$; Roosting : $b = \frac{1}{20}$; Propulsion : $\alpha = 0.07, \beta = 0.05$).

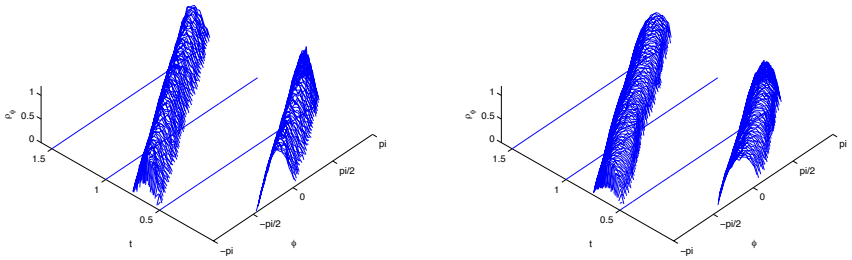

(a) Microscopic (b) Hydrodynamic

Figure 7: Angular densities for a milling flock. The angular velocity of the flock is given by the averaged particle circumference per equilibrium speed (Interaction: $C_A = 20$, $C_R = 50$, $l_A = 100$, $l_R = 2$; Roosting : $b = \frac{1}{20}$, $R_{\text{Roost}} = 30$; Propulsion : $\alpha = 0.07, \beta = 0.05$).

well with microscopic simulations. The only difference is, that the hydrodynamic density is nonzero for small r outside the microscopic mill, but this is due to smoothing properties of the hydrodynamic method. Figure 6 illustrates, how single mills are compressed in radial densities. Therefore, the hydrodynamic equation yield the same mill shrinking for roosting, as the microscopic simulation in figure 4.

In figure 7, we show the evolution of the radial density $\rho_\varphi(\varphi) = \int r\rho(r,\varphi)\mathrm{d}r$ for the milling flock of type figure 5(a). The time is rescaled to $\tilde{t} := t/(2\pi\bar{r}\sqrt{\alpha/\beta})$, where $\tilde{r}$ is the averaged radius of particles. The milling flock travels at constant speed with angular speed matching the flocks average circumference per equilibrium speed. Microscopic and hydrodynamic simulation are an almost perfect match. In particular, the support of the angular density is not enlarged in the hydrodynamic simulation for this scenario.

Remark 5.1. *We remark, that the simulated radial densities of single mills are numerically verified solutions of the integral equation (4.9), which in presence of roosting contains the roosting potential on the right hand side. The monokinetic ansatz used to derive the integral equation is indeed numerically fulfilled by the microscopic and hydrodynamic simulations. Interlaced rotations as in figure 5(c) can not be observed in the monokinetic hydrodynamics.*

6. Concluding Remarks

The model for self-propelled interacting particles in [CDMBC07] or [CDP09] has been extended to include a roosting behavior of the individuals. The resulting equations have been investigated numerically and analytically. Several asymptotic limits have been considered and reduced diffusive and

hyperbolic approximations have been derived. The roosting term forces particles to turn back to a preferred area, as being motivated from biological models. We have studied effects of the roosting force on patterns known from pure attraction-repulsion scenarios, as well as new collective behaviors like milling flocks. Though the formation of such patterns is verified also in hydrodynamic simulation, a categorization of initial conditions, parameters, and resulting collective behavior is unknown at present state.

Acknowledgment. JAC acknowledges support from the project MTM2008-06349-C03-03 DGI-MCI (Spain) and 2009-SGR-345 from AGAUR-Generalitat de Catalunya. The work of the last three authors has been supported by DFG grant KL 1105/17-1 and KL 1105/18-1.

References

[BCCCCGLOPPVZ09] Ballerini, M., Cabibbo, N., Candelier, R., Cavagna, A., Cisbani, E., Giardina, L., Lecomte, L., Orlandi, A., Parisi, G., Procaccini, A., Viale, M., Zdravkovic, V.: Interaction ruling animal collective behavior depends on topological rather than metric distance: evidence from a field study. Preprint.

[BTTYB09] Barbaro, A., Taylor, K., Trethewey, P.F., Youseff, L., Birnir, B.: Discrete and continuous models of the dynamics of pelagic fish: application to the capelin. Mathematics and Computers in Simulation, **79**, 3397–3414 (2009)

[BEBSVPSS09] Barbaro, A., Einarsson, B., Birnir, B., Sigurthsson, S., Valdimarsson, H., Palsson, O.K., Sveinbjornsson, S., Sigurthsson, T.: Modelling and simulations of the migration of pelagic fish. ICES J. Mar. Sci., **66**, 826–838 (2009)

[BCC] Bolley, F., Canizo, J.A., Carrillo, J.A.: Propagation of chaos for some non-globally Lipschitz particle systems. Preprint UAB

[BDT99] Bonabeau, E., Dorigo, M., Theraulaz, G.: Swarm Intelligence: From Natural to Artificial Systems. Oxford University Press, New York (1999)

[BGKMW07] L. Bonilla, T. Götz, A. Klar, N. Marheineke, R. Wegener. Hydrodynamic limit for the Fokker–Planck equation of fiber lay–down models. SIAM Appl. Math. 2007

[BH77] Braun, W., Hepp, K.: The Vlasov Dynamics and Its Fluctuations in the 1/N Limit of Interacting Classical Particles. Commun. Math. Phys., **56**, 101–113 (1977)

[BCM07] Burger, M., Capasso, V., Morale, D.: On an aggregation model with long and short range interactions. Nonlinear Analysis. Real World Applications. An International Multidisciplinary Journal, **8**, 939–958 (2007)

[CDFSTB03] Camazine, S., Deneubourg, J.-L., Franks, N.R., Sneyd, J., Theraulaz, G., Bonabeau, E.: Self-Organization in Biological Systems. Princeton University Press (2003)

[CCR09] Cañizo, J.A., Carrillo, J.A., Rosado, J.: A well-posedness theory in measures for some kinetic models of collective motion. Preprint UAB.

[CCR10] J. A. Cañizo, J. A. Carrillo, J. Rosado, Collective Behavior of Animals: Swarming and Complex Patterns, to appear in Arbor.

[CDP09] Carrillo, J.A., D'Orsogna, M.R., Panferov, V.: Double milling in self-propelled swarms from kinetic theory. Kinetic and Related Models, **2**, 363-378 (2009)

[CFRT09] Carrillo, J.A., Fornasier, M., Rosado, J., Toscani, G.: Asymptotic Flocking Dynamics for the kinetic Cucker-Smale model. to appear in SIAM J. Math. Anal.

[CFTV10] J. A. Carrillo, M. Fornasier, G. Toscani, F. Vecil, Particle, Kinetic, and Hydrodynamic Models of Swarming, Preprint UAB.

[CHDB07] Chuang, Y.L., Huang, Y.R., D'Orsogna, M.R., Bertozzi, A.L.: Multi-vehicle flocking: scalability of cooperative control algorithms using pairwise potentials. IEEE International Conference on Robotics and Automation, 2292–2299 (2007)

[CDMBC07] Chuang, Y.L., D'Orsogna, M.R., Marthaler, D., Bertozzi, A.L., Chayes, L.: State transitions and the continuum limit for a 2D interacting, self-propelled particle system. Physica D, **232**, 33–47 (2007)

[CKFL05] Couzin, I.D., Krause, J., Franks, N.R., Levin, S.A.: Effective leadership and decision making in animal groups on the move. Nature, **433**, 513–516 (2005)

[CKJRF02] Couzin, I.D., Krause, J., James, R., Ruxton, G. and Franks, N.: Collective memory and spatial sorting in animal groups. Journal of Theoretical Biology, **218**, 1–11 (2002)

[DM08] Degond, P., Motsch, S.: Continuum limit of self-driven particles with orientation interaction. Math. Models Methods Appl. Sci., **18**, 1193–1215 (2008)

[DV01] L. Desvilettes, C. Villani. On the trend to global equilibrium for spatially inhomogeneous entropy-dissipating systems: the linear Fokker–Planck equation. *Comm. Pure Appl. Math.*, 54:1–42, 2001.

[Dou79] Dobrushin, R.: Vlasov equations. Funct. Anal. Appl., **13**, 115–123 (1979)

[DCBC06] D'Orsogna, M.R., Chuang, Y.L., Bertozzi, A.L., Chayes, L.: Self-propelled particles with soft-core interactions: patterns, stability, and collapse. Phys. Rev. Lett., **96** (2006)

[GKMW07] T. Götz, A. Klar, N. Marheineke, R. Wegener. A stochastic model and associated Fokker–Planck equation for the fiber lay-down process in nonwoven production processes. SIAM Appl. Math, 2007

[GC04] Grégoire, G., Chaté, H.: Onset of collective and cohesive motion. Phy. Rev. Lett., **92** (2004)

[HL09] Ha, S.-Y., Liu, J.-G.: A simple proof of the Cucker-Smale flocking dynamics and mean-field limit. Comm. Math. Sci., **7**, 297-325 (2009)

[HT08] Ha, S.-Y., Tadmor, E.: From particle to kinetic and hydrodynamic descriptions of flocking. Kinetic and Related Models, **1**, 415–435 (2008)

[HK05] Hemelrijk, C.K. and Kunz, H.: Density distribution and size sorting in fish schools: an individual-based model. Behavioral Ecology, **16**, 178–187 (2005)

[HKMO09] Herty,M., Klar, A., Motsch,S., Olawsky,F.: A smooth model for fiber lay-down processes and its diffusion approximations, KRM 2 (3), 480-502, (2009)

[HCH] Hildenbrandt, H, Carere, C., and Hemelrijk, C. K.: Self-organised complex aerial displays of thousands of starlings: a model.

[HW92] Huth, A. and Wissel, C.: The Simulation of the Movement of Fish Schools. Journal of Theoretical Biology (1992)

[KRS07] A. Klar, P. Reuterswärd, M. Seaïd. A semi-Lagrangian method for the Fokker–Planck equation of fiber dynamics. JSC, 2009

[KH03] Kunz, H. and Hemelrijk, C. K. 2003: Artificial fish schools: collective effects of school size, body size, and body form. Artificial Life, 9(3):237253.

[LRC00] Levine, H., Rappel, W.J., Cohen, I.: Self-organization in systems of self-propelled particles. Phys. Rev. E, **63** (2000)

[LLE08a] Li, Y.X., Lukeman, R., Edelstein-Keshet, L.: Minimal mechanisms for school formation in self-propelled particles. Physica D, **237**, 699–720 (2008)

[LLE08b] Li, Y.X., Lukeman, R., Edelstein-Keshet, L.: A conceptual model for milling formations in biological aggregates. Bull Math Biol., **71**, 352–382 (2008)

[MEBS03] Mogilner, A., Edelstein-Keshet, L., Bent, L., Spiros, A., Mutual interactions, potentials, and individual distance in a social aggregation. J. Math. Biol., **47**, 353–389 (2003)

[Neu77] Neunzert, H.: The Vlasov equation as a limit of Hamiltonian classical mechanical systems of interacting particles. Trans. Fluid Dynamics, **18**, 663–678 (1977)

[PE99] Parrish, J., Edelstein-Keshet, L.: Complexity, pattern, and evolutionary trade-offs in animal aggregation. Science, **294**, 99–101 (1999)

[Ri89] Risken, H.: The Fokker-Planck equation, Springer Series in Synergetics 18, Springer-Verlag 1989.

[Szn91] Sznitman, A.-S.: Topics in propagation of chaos, École d'Été de Probabilités de Saint-Flour XIX—1989, Lecture Notes in Math. 1464, 165–251, Springer, 1991.

[Spo91] Spohn, H.: Large scale dynamics of interacting particles. Texts and Monographs in Physics, Springer (1991)

[TK07] S. Tiwari, J. Kuhnert, J. Comp. Appl. Math., 203, 2007. Modelling of two-phase flow with surface tension by Finite Point-set method (FPM). J. Comp. Appl. Math., 203, 2007

[TT95] Toner, J., Tu, Y.: Long-range order in a two-dimensional dynamical xy model: How birds fly together. Phys. Rev. Lett., **75**, 4326–4329 (1995)

[TB04] Topaz, C.M., Bertozzi, A.L.: Swarming patterns in a two-dimensional kinematic model for biological groups. SIAM J. Appl. Math., **65**, 152–174 (2004)

[TBL06] Topaz, C.M., Bertozzi, A.L., Lewis, M.A.: A nonlocal continuum model for biological aggregation. Bulletin of Mathematical Biology, **68**, 1601–1623 (2006)

[VCBCS95] Vicsek, T., Czirok, A., Ben-Jacob, E., Cohen, I., Shochet, O.: Novel type of phase transition in a system of self-driven particles, Phys. Rev. Lett., **75**, 1226–1229 (1995)

J. A. Carrillo, ICREA - Departament de Matemàtiques, Universitat Autònoma de Barcelona, 08193 Bellaterra, Spain.
Email: carrillo@mat.uab.es,
A.Klar, Department of Mathematics, University of Kaiserslautern,
P.O.Box 3049, 67653 Kaiserslautern, Germany; Fraunhofer ITWM Kaiserslautern, 67663 Kaiserslautern, Germany
Email: klar@mathematik.uni-kl.de,
S. Martin, Department of Mathematics, University of Kaiserslautern,
P.O.Box 3049, 67653 Kaiserslautern, Germany.
Email: smartin@mathematik.uni-kl.de,
S. Tiwari, Department of Mathematics, University of Kaiserslautern,
P.O.Box 3049, 67653 Kaiserslautern, Germany.
Email: tiwari@mathematik.uni-kl.de,